Electronic Supplementary Material (ESI) for Physical Chemistry Chemical Physics.

Supplementary material

Experimental verification of chemical "neurocomputer"

Ivan S. Proskurkin, [a] Pavel S. Smelov [b] and Vladimir K. Vanag *[c]

Centre for Nonlinear Chemistry, Immanuel Kant Baltic Federal University, Kaliningrad, 236041, Russia.

Table S.1. Phases of the CPG micro-oscillators at which they should be perturbed for the mode switching.

	IP	AP	W	WR
IP		$\varphi_{sw}^{(10)} = 0.7$ $\varphi_{sw}^{(12)} = 0.7$ $\Delta t_{sw} = 8$ s	$\varphi_{sw}^{(10)} = 0.26$ $\varphi_{sw}^{(11)} = 0.7$ $\varphi_{sw}^{(12)} = 0.92$ $\Delta t_{sw} = 8$ s	$\varphi_{sw}^{(10)} = 0.92$ $\varphi_{sw}^{(11)} = 0.85$ $\varphi_{sw}^{(12)} = 0.65$ $\Delta t_{sw} = 10$ s
AP	$\varphi_{sw}^{(10)} = 0.7$ $\varphi_{sw}^{(12)} = 0.7$ $\Delta t_{sw} = 8$ s		$\varphi_{sw}^{(10)} = 0.75$ $\varphi_{sw}^{(11)} = 0.87$ $\varphi_{sw}^{(12)} = 0.61$ $\Delta t_{sw} = 8$ s	$\varphi_{sw}^{(11)} = 0.7$ $\varphi_{sw}^{(12)} = 0.9$ $\Delta t_{sw} = 10$ s
W	$\varphi_{sw}^{(10)} = 0.92$ $\varphi_{sw}^{(11)} = 0.69$ $\varphi_{sw}^{(12)} = 0.81$ $\Delta t_{sw} = 13$ s	$\varphi_{sw}^{(10)} = 0.34$ $\varphi_{sw}^{(11)} = 0.8$ $\varphi_{sw}^{(12)} = 0.88$ $\Delta t_{sw} = 13$ s		
WR	$\varphi_{sw}^{(10)} = 0.26$ $\varphi_{sw}^{(11)} = 0.65$ $\varphi_{sw}^{(12)} = 0.92$ $\Delta t_{sw} = 8$ s	$\varphi_{sw}^{(11)} = 0.94$ $\varphi_{sw}^{(12)} = 0.91$ $\Delta t_{sw} = 10$ s		

The left column presents the initial modes of the CPG, while the first row presents the final modes after transition. Durations of switching pulses Δt_{sw} are different for different transitions. Superscript k in $\varphi_{sw}^{(k)}$ (k = 10, 11, 12) means the index of a CPG cell which receives a pulsed perturbation. Gray cells for the WR $\rightarrow$ W and W $\rightarrow$ WR transitions mean that these modes do not coexist at the same parameters. Among the phases $\varphi_{sw}^{(k)}$, there are many values which are close to 0.9. This is explained by the fact that the sensitivity of the BZ cells to a perturbation measured as $\Delta\varphi_k$ increases with $\varphi_{sw}^{(k)}$. The desired phases $\varphi_{sw}^{(k)}$ can vary in the ranges $\varphi_{sw}^{(k)}(1 \pm 0.2)$ for $\varphi_{sw}^{(k)} < 0.35$, $\varphi_{sw}^{(k)}(1 \pm 0.05)$ for $0.6 < \varphi_{sw}^{(k)} < 0.75$, and $\varphi_{sw}^{(k)}(1 \pm 0.01)$ for $0.75 < \varphi_{sw}^{(k)}$, where $\varphi_{sw}^{(k)}$ are the values given in Table I. Note also, if we increase duration Δt_{sw}, the phases $\varphi_{sw}^{(k)}$ can be decreased and *vice versa*.

Switching between the CN modes

To prove that our CN works well, we demonstrate all the transitions between the four internal CPG modes induced by modes in the antenna unit. In Fig. S.1, we group two transitions, the IP → W and the IP → WR. In Fig. S.2, we present all the transitions from the AP mode: the AP → IP transition, the AP → W, and the AP → WR. In Fig. S.3, the two transitions from the W mode are shown: W → IP and W → AP. And finally in Fig. S.4, the two transitions, WR → IP and WR → AP are exhibited.

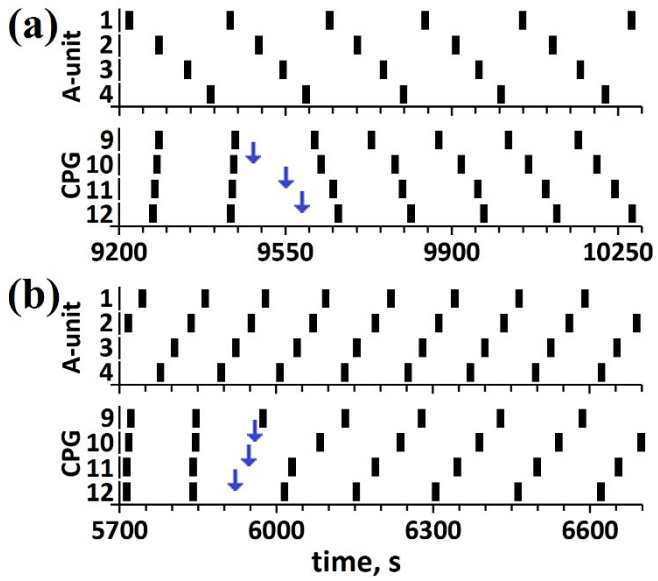

Figure S.1. (**a**) Kinetics of the IP → W transition. Parameters in the A-unit: τ_A = 25 s, Δt_A = 18 s, T = 210 s; in the CPG: τ_{CPG} = 80 s, Δt_{CPG} = 7 s, T = 164 s. Parameters for the switching pulses: $\varphi_{sw}^{(10)}$ = 0.26, $\varphi_{sw}^{(11)}$ = 0.7, $\varphi_{sw}^{(12)}$ = 0.92, Δt_{sw} = 8 s. (**b**) Kinetics of the IP → WR transition. Parameters in the A-unit: τ_A = 55 s, Δt_A = 18 s, T = 119 s; in the CPG: τ_{CPG} = 40 s, Δt_{CPG} = 7 s, T = 126 s. Parameters for the switching pulses: $\varphi_{sw}^{(10)}$ = 0.92, $\varphi_{sw}^{(11)}$ = 0.85, $\varphi_{sw}^{(12)}$ = 0.65, Δt_{sw} = 10 s.

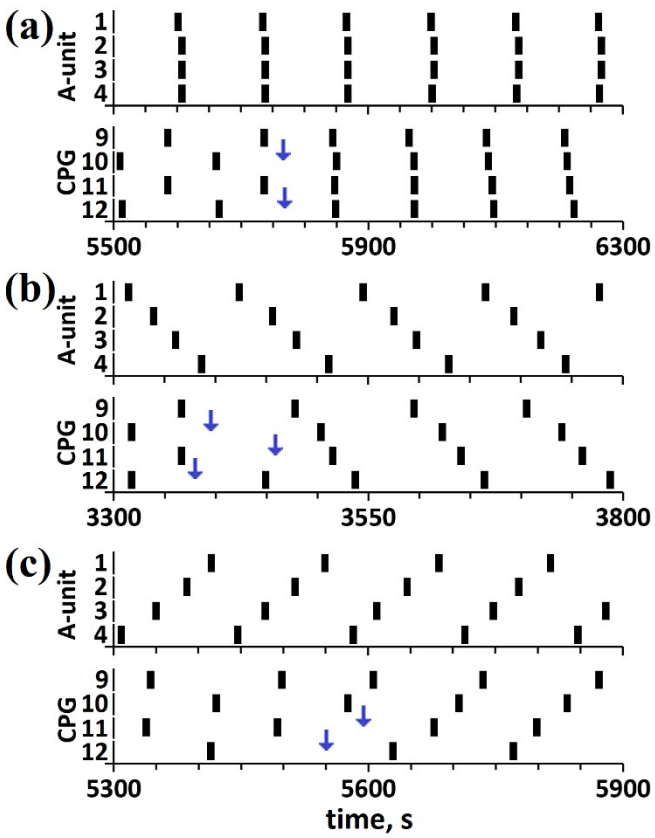

Figure S.2. (**a**) Kinetics of the AP → IP transition. Parameters in the A-unit: τ_A = 102 s, Δt_A = 18 s, T = 130 s; in the CPG: τ_{CPG} = 10 s, Δt_{CPG} = 7 s, T = 153 s. Parameters for the switching pulses: $\varphi_{sw}^{(10)} = \varphi_{sw}^{(12)}$ = 0.7, Δt_{sw} = 8 s. (**b**) Kinetics of the AP → W transition. Parameters in the A-unit: τ_A = 25 s, Δt_A = 18 s, T = 205 s; in the CPG: τ_{CPG} = 80 s, Δt_{CPG} = 7 s, T = 107 s. Parameters for the switching pulses: $\varphi_{sw}^{(10)}$ = 0.75, $\varphi_{sw}^{(11)}$ = 0.87, $\varphi_{sw}^{(12)}$ = 0.61, Δt_{sw} = 8 s. (**c**) Kinetics of the AP → WR transition. Parameters in the A-unit: τ_A = 55 s, Δt_A = 18 s, T = 120 s; in the CPG: τ_{CPG} = 10 s, Δt_{CPG} = 7 s, T = 151 s. Parameters for the switching pulses: $\varphi_{sw}^{(11)}$ = 0.7, $\varphi_{sw}^{(12)}$ = 0.9, Δt_{sw} = 10 s.

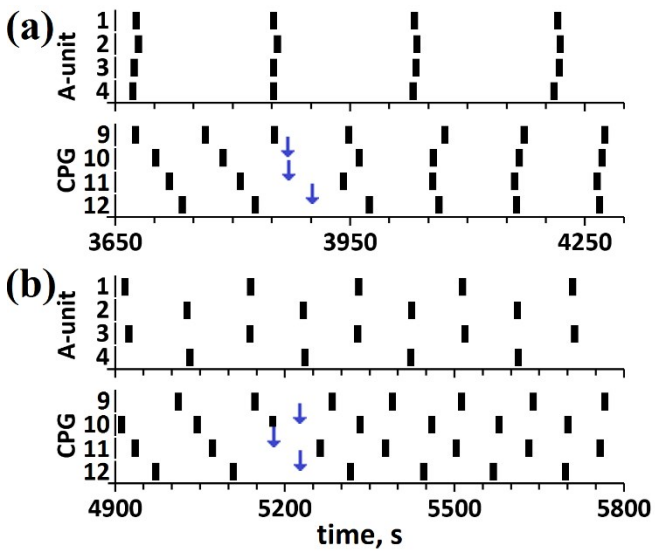

Figure S.3. (**a**) Kinetics of the W → IP transition. Parameters in the A-unit: τ_A = 160 s, Δt_A = 18 s, T = 178 s; in the CPG: τ_{CPG} = 45 s, Δt_{CPG} = 7 s, T = 90 s. Parameters for the switching pulses: $\varphi_{sw}^{(10)}$ = 0.92, $\varphi_{sw}^{(11)}$ = 0.69, $\varphi_{sw}^{(12)}$ = 0.81, Δt_{sw} = 12.5 s. (**b**) Kinetics of the W → AP transition. Parameters in the A-unit: τ_A = 60 s, Δt_A = 18 s, T = 215 s; in the CPG: τ_{CPG} = 100 s, Δt_{CPG} = 7 s, T = 136 s. Parameters for the switching pulses: $\varphi_{sw}^{(10)}$ = 0.34, $\varphi_{sw}^{(11)}$ = 0.8, $\varphi_{sw}^{(12)}$ = 0.88, Δt_{sw} = 13 s.

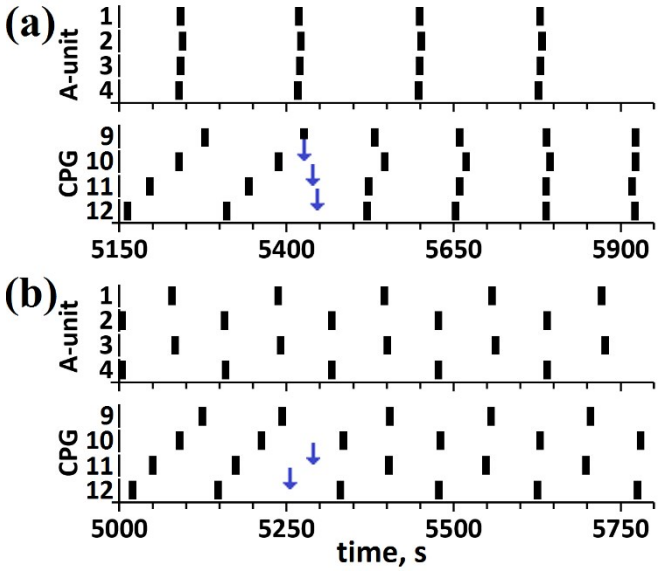

Figure S.4. (**a**) Kinetics of the WR → IP transition. Parameters in the A-unit τ_A = 160 s, Δt_A = 18 s, T = 179 s; in the CPG: τ_{CPG} = 40 s, Δt_{CPG} = 7 s, T = 148 s. Parameters for the switching pulses: $\varphi_{sw}^{(10)}$ = 0.26, $\varphi_{sw}^{(11)}$ = 0.65, $\varphi_{sw}^{(12)}$ = 0.92, Δt_{sw} = 8 s. (**b**) Kinetics of the WR → AP transition. Parameters in the A-unit: τ_A = 50 s, Δt_A = 18 s, T = 157 s; in the CPG: τ_{CPG} = 10 s, Δt_{CPG} = 7 s, T = 123 s. Parameters for the switching pulses: $\varphi_{sw}^{(11)}$ = 0.94, $\varphi_{sw}^{(12)}$ = 0.91, Δt_{sw} = 10 s.

The IP → AP transition for the CN with R- and R_A electronic units

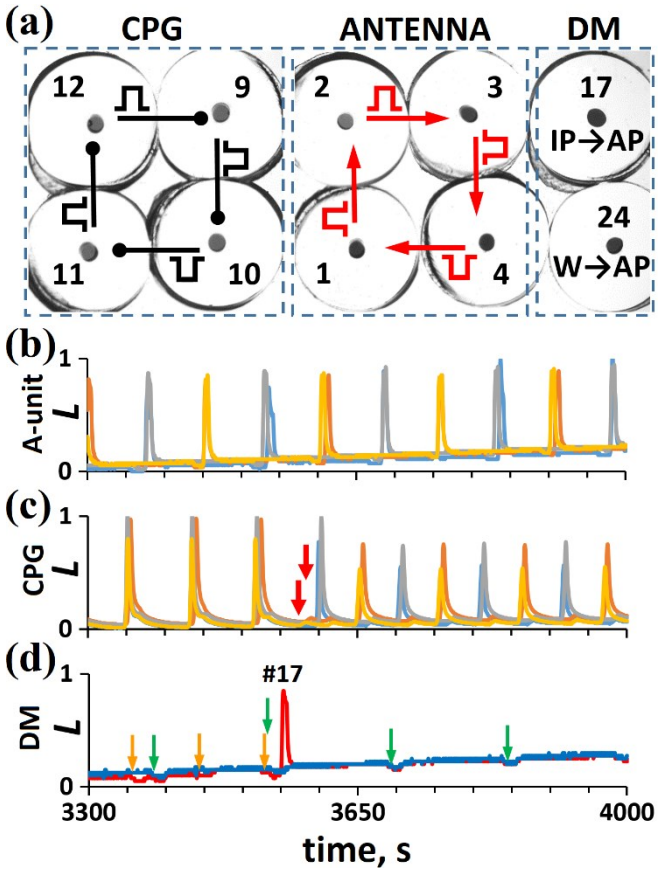

Figure. S.5. The IP → AP transition for a hybrid CN with electronic R- and R_A units, while the CPG, antenna, and DM units are made of BZ micro-cells. The CPG cells are coupled via inhibitory pulses, while A-cells are coupled via excitatory "negative" pulses. Both coupling is unidirectional. For the IP → AP transition, only one BZ cell in the DM unit, cell #17, is used. Electronic R- and R_A units are not shown in Fig. S.5, but they are the same as in Fig. 6(a). The coupling between all CN units is as in Fig. 5 as well. The DM unit receives pulses from the readers R- and R_A [orange and green arrows in panel (d)]. These pulses indicate that the CPG is in the IP mode, while the A-unit is in the AP mode. Kinetics of the CPG cells [panel (b) at $t < 3600$ s] and A-cells [panel (c)] confirm this. At $t \cong 3540$ s, both pulses from the R- and R_A units come to the DM cell #17 simultaneously. These simultaneous pulses trigger spike in cell #17, which in turn generates switching pulses (with delays $\tau_{sw}^{(10)} = 29$ s, $\tau_{sw}^{(12)} = 22$ s) that come to diagonal CPG cells #10 and #12 at $t \cong 3580$ s. The last pulses switch the CPG from the IP to AP mode. Green arrows in panel (d) at $t > 3650$ s indicate moments of time when pulses from the R_A unit come to cells #17 and #24, but these pulses cannot generate a spike, since two simultaneous pulses are needed for this.